View Article Online
View Journal

Dalton Transactions

An international journal of inorganic chemistry

Accepted Manuscript

This article can be cited before page numbers have been issued, to do this please use: Y. Song, M. Kong, X. Feng, J. Li, Z. Hu, J. Wang, X. Song, Z. Jing and Y. Zhang, *Dalton Trans.*, 2020, DOI: 10.1039/D0DT02864A.

ROYAL SOCIETY OF CHEMISTRY

rsc.li/dalton

View Article Online
DOI: 10.1039/D0DT02864A

ARTICLE

Structurally modulated single-ion magnets of mononuclear β-diketone dysprosium(III) complexes†

Received 00th January 20xx,
Accepted 00th January 20xx

DOI: 10.1039/x0xx00000x

Ming Kong,[a] Xin Feng, [a] Jing Li, [a] Zhao-Bo Hu, [a] Jia Wang, [a] Xiao-Jiao Song, [a] Zhao-Yang Jing, [a] Yi-Quan Zhang,*[b] and You Song*[a]

Five β-diketone based Dy(III) single-ion magnets (SIMs) of $[Dy^{III}(TTA)_3(AIP)]\cdot 0.5CH_3CH_2OH\cdot 0.5H_2O$ (**1**), $[Dy^{III}(TTA)_3(APIP)]\cdot 2CH_3OH\cdot H_2O$ (**2**), $[Dy^{III}(TTA)_3(DPP)]$ (**3**), $[Dy^{III}(TTA)_3(BPP)]\cdot 0.5CH_3CH_2OH$ (**4**) and $[Dy^{III}(TTA)_3(AIP)]\cdot 1.5H_2O$ (**5**), have been fully synthesized through alteration of the phenanthroline derivates (AIP = 2-(anthracen-9-yl)-1H-imidazo[4,5-f][1,10]phenanthroline, APIP = 2-(4-(anthracen-9-yl)phenyl)-1H-imidazo[4,5-f][1,10]phenanthroline, DPP = 2,3-diphenylpyrazino[2,3-f][1,10]phenanthroline and BPP = 2,3-bis(2,5-dimethylthiophen-3-yl)pyrazino[2,3-f][1,10]phenanthroline). Magnetic investigations reveal that all complexes perform as SIMs with notably different effective barriers of 69.4 K (**1**), 147.3 K (**2**), 122.1 K (**3**) and 234.2 K (**4**) in zero direct current (dc) field. Complexes of **2** and **4** possess almost twofold higher effective barriers than the comparative **1** and **3**. By the analyzing the crystal structures, the distinction of magnetic dynamic stems from the variation of intermolecular hydrogen bonds interaction and charge delocalization of auxiliary ligands. With the help of *ab initio* calculation, the conspicuous variation of auxiliary ligand brings about varying intensity of quantum tunnelling magnetization (QTM), which accounts for the distinguishable magnetic dynamic. With the combination of experimental and theoretical analyses, this work provides a visual and instructive perspective to the understanding of the authenticity of fine tuning of auxiliary ligand for designing such structurally modulated SIMs of mononuclear β-diketone Dysprosium(III) complexes.

Introduction

The lanthanide single-ion magnets (Ln(III)-SIMs), displaying slow relaxation of magnetization as an important member of single molecule magnets (SMMs), have raised worldwide attention for their significant single-ion magnetic anisotropy. Such property is rooted in large unquenched orbital angular momentum and intrinsic strong spin orbit coupling of lanthanide ions, especially Dy(III), Tb(III) and Er(III) ions.[1-3] In addition, further understanding of magneto-structural correlations contributes to the explanation between macroscopic magnetic properties and the quantum effects in SMMs. Recently, the development of Dy(III)-based SIMs with high anisotropy barrier that aiming at maximum relaxation energy barrier and the highest blocking temperature is of great interest for their potential applications of high density data storage, quantum computation and spintronics.[4-10] The top trend towards the goal now is to control the symmetry of lanthanide ions.[11] Considering a large magnetic anisotropy barrier for SIMs, the anisotropic Kramers ion Dy(III) is a good candidate for its large m_J (15/2) and degenerate ground states. In the past, numerous studies on high-performance SIMs have manifested that the highly symmetrical Dy(III)-based SIMs, such as D_{4d}, D_{5h} and D_{6h}, can minimize the electron repulsion around the lanthanide ion and stabilize the m_J = ±15/2 state to avoid quantum tunnelling magnetization (QTM).[12-20]

The structures with approximate square-antiprismatic or dodecahedron coordination polyhedron are of great interest owing to the promising application in constructing SIMs and facile synthesis.[13] Such SIMs have demonstrated that subtle modification by lattice solvents, auxiliary ligand and intermolecular interaction usually result in the distortion of coordination-sphere and thus bring out distinct magnetic relaxation behavior.[16,21,23b] Thus, the series of eight-coordinate Dy-β-diketones complexes of [Ln(β-diketone)$_3$L] have been extensively used to construct high-performance Dy(III) SIMs through regulation of the auxiliary ligands.[22,23] As building block for linking phenanthroline ligand, the protonated five-membered imidazole ring and non-protonated six-membered pyrazine ring has been confirmed as effective groups to regulate intermolecular hydrogen bond and transmit charge conjugation effects.[12,23d] Therefore, these types of complexes containing bridged imidazole or pyrazine moiety can efficiently modulate the magnetic structure of lanthanide-based SIMs.

[a] *State Key Laboratory of Coordination Chemistry, School of Chemistry and Chemical Engineering, Collaborative Innovation Center of Advanced Microstructure, Nanjing University, Nanjing 210023, People's Republic of China.*
[b] *Jiangsu Key Lab For NSLSCS, School of Physical Science and Technology, Nanjing Normal University, Nanjing 210023, People's Republic of China.*

† Electronic Supplementary Information (ESI) available: Synthetic procedure, crystallographic relative data, SHAPE analysis, PXRD and magnetic relative data, calculated results. CCDC 1994048 and 1994050-1994052, 2033641. For ESI and crystallographic data in CIF or other electronic format see DOI: 10.1039/x0xx00000x

Scheme 1. Schematic chemical structure of complexes **1**-**4**.

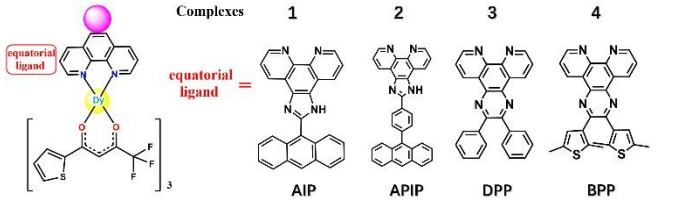

There has been evidence that the local symmetry of Dy(III) ions plays a key role in modulating the single-ion anisotropy.[11] Meanwhile, the electron-donating or -withdrawing effect of auxiliary ligands that indirectly influences the electrostatic potential (ESP) around the central Dy(III) ions, is also the decisive factor to regulate the magnetic dynamic, especially in facilitating the suppression of fast relaxation. According to previous report, it has been proven that the notional electron-withdrawing effect of β-diketone results in the reduction of magnetic relaxation barriers.[24] Therefore, how electron effect of auxiliary ligand influences the magnetic dynamic are indeed necessary to completely explore.

Herein, we present four Dy-β-diketones complexes based on phenanthroline ligand with different electron-donating groups linked by imidazole or pyrazine moiety, that is, [Dy(TTA)$_3$AIP] (**1**), [Dy(TTA)$_3$APIP] (**2**), [Dy(TTA)$_3$DPP] (**3**), and [Dy(TTA)$_3$BPP] (**4**) (Scheme 1). The Dy(III) centre with eight-coordination environment of N_2O_6 bear the distorted square-antiprismatic or triangular dodecahedron geometry. The magnetic relaxation studies and CASSCF/SI-SO calculations indicated that these properties can be modified by the slightly modulated auxiliary phenanthroline ligands.

Experimental

Materials and methods

All chemicals and solvents are commercially available and used without further purification. The ligands of DPP and BPP are synthesized by the cyclization combining 1,10-phenanthroline-5,6-diamine with corresponding 1,2-dione.[25,26] The other two ligands, AIP and APIP, are synthesized by a similar ring closing reaction using corresponding aromatic carbaldehyde and phenanthroline-5,6-dione (Scheme S1†). Elemental analyses of C, H and N were recorded on a PerkinElmer 240C elemental analyzer. ^{1}H-NMR and MALDI-TOF-MS data were obtained on Bruker Advance III 500 MHz nuclear resonance spectrometers and Bruker ultraflex treme TOF/TOF.

X-ray Crystallography

The single-crystal X-ray measurements of **1**-**4** were carried out on a Bruker D8 venture diffractometer fitted with a PHOTON-100 COMS detector with Mo Kα radiation (λ = 0.71073 Å) by using an ω scan mode at 153 K. The diffraction data were treated using SAINT, and all absorption corrections were carried out by using SADABS. All non-hydrogen atoms were labelled by Patterson's method using the SHELXS programs of the SHELXTL package and by subsequent difference Fourier syntheses. The all hydrogens were determined theoretically and refined with isotropic thermal parameters riding on their parents. All non-hydrogen atoms were refined by a full-matrix least-squares technique based on F^2. All calculations were performed by SHELXTL-97.[27-29]

View Article Online DOI: 10.1039/D0DT02641A

Magnetic Measurements

The alternating current (ac) magnetic susceptibility data were collected using a PPMS (**1** and **2**) or MPMS (**3**, **4** and **5**) magnetometer with an ac field of 5 Oe or 2 Oe in the frequencies ranging from 1 to 10000 or 1-999 Hz respectively. The direct current (dc) magnetic susceptibility data of **1**-**5** were measured in the temperature range from 1.8 to 300 K using MPMS magnetometer. Experimental susceptibilities were corrected for the diamagnetism of the samples as estimated from Pascal's tables and of the sample holder by a previous calibration.[30]

Ab initio Calculations

Complete-active-space self-consistent-field (CASSCF) calculations based on the experimental single crystal X-ray data were performed with the MOLCAS 8.4 program package on individual Dy(III) fragment for each complex. For CASSCF calculations, the basis sets used are atomic natural orbitals from the MOLCAS ANO-RCC library: ANO-RCC-VTZP for Dy(III) ion; VTZ for close O and N; VDZ for distant atoms. The calculations employed the second order Douglas-Kroll-Hess Hamiltonian, where scar relativistic contractions were taken into account in the basis set and the spin-orbit coupling were handled separately in the restricted active space state (RASSI-SO) procedure. The active electrons in seven active spaces contain all *f* electrons CAS (9 in 7) for each Dy(III) fragment. The maximum number of spin-free states that are possible with our hardware include all 21 sextets, 128 from 224 quadruplets, and 130 from 490 doublets for Dy(III) fragment.[31]

Synthesis of AIP and APIP. The synthesis route of AIP and APIP is similar and here AIP as an example showed below. In a 100 mL round bottom flask, 1.03 g (5 mmol) of anthracene-9-carbaldehyde and 1.05 g (5 mmol) of 1,10-phenanthroline-5,6-dione are mixed and then 5.00 g of ammonium acetate is added meanwhile together with 40 mL of glacial acetic acid. The solvent was removed after refluxing overnight and poured in water accompanied with yellow precipitate. After the filtration and evaporation, the target product was further purified by recrystallization in ethanol, yielding a yellow power (1.79 g, 86%). APIP: The target product was further purified by recrystallization in ethanol, yielding a yellow power (1.81 g, 75%). AIP: MALDI-TOF-MS (*m*/*z*) Calcd. for $C_{27}H_{16}N_4$: 396.14, found 397.320. ^{1}H-NMR (500 MHz, DMSO-*d*6) δ 14.22 (s, 1H), 9.10 (dd, *J* = 4.3, 1.8 Hz, 2H), 8.97 (dd, *J* = 8.0, 1.8 Hz, 1H), 8.93 (s, 1H), 8.79 (dd, *J* = 8.2, 1.7 Hz, 1H), 8.28 (*d*, *J* = 8.4 Hz, 2H), 7.89 –7.78 (m, 4H), 7.63 (ddd, *J* = 8.4, 6.5, 1.2 Hz, 2H), 7.56 (ddd, *J* = 8.8, 6.5, 1.3 Hz, 2H). APIP: MALDI-TOF-MS (*m*/*z*) Calcd. for $C_{33}H_{20}N_4$: 472.17, found 473.344. ^{1}H-NMR (500 MHz, DMSO-*d*6)

View Article Online
DOI: 10.1039/D0DT02864A

δ 13.97 (s, 1H), 9.09 (dd, *J* = 7.6, 1.8 Hz, 1H), 9.09 (s, 1H), 9.01 (ddd, *J* = 8.2, 3.9, 1.7 Hz, 2H), 8.75 (s, 1H), 8.60 – 8.54 (m, 2H), 8.21 (d, *J* = 8.5 Hz, 2H), 7.90 (ddd, *J* = 25.0, 8.2, 4.3 Hz, 2H), 7.74 – 7.64 (m, 4H), 7.58 (ddd, *J* = 8.3, 6.5, 1.1 Hz, 2H), 7.50 (ddd, *J* = 8.0, 6.5, 1.3 Hz, 2H).

Synthesis of DPP and BPP. The synthesis routes of DPP and BPP are similar and here BPP as an example showed below. In a 100 mL round bottom flask, 1.05 g (5 mmol) of 1,10-phenanthroline-5,6-diamine and 1.50 g (5.4 mmol) of 1,2-bis(2,5-dimethylthiophen-3-yl) ethane-1,2-dione are mixed, and then 25 mL methanol is subsequently added together with 25 mL of glacial acetic acid. The solvents are removed after refluxing for 10 hours and poured in water accompanied with white precipitate. After the filtration and evaporation, the target product was further purified by flash chromatography, yielding a white power (1.90 g, 77.5%). DPP: The target product was further purified by recrystallization in ethanol, yielding a yellow power (77%). DPP: MALDI-TOF-MS (*m/z*) Calcd. for $C_{26}H_{16}N_4$: 384.14, found 385.326. ^{1}H-NMR (500 MHz, DMSO-*d*6) *δ* 9.52 (dd, *J* = 8.1, 1.8 Hz, 2H), 9.26 (dd, *J* = 4.3, 1.8 Hz, 2H), 7.98 (dd, *J* = 8.1, 4.3 Hz, 2H), 7.73 – 7.67 (m, 4H), 7.52 – 7.40 (m, 6H). BPP: MALDI-TOF-MS (m/z) Calcd. For $C_{26}H_{20}N_4S_2$: 452.11, found 453.286. ^{1}H-NMR (500 MHz, DMSO-*d*6) *δ* 9.43 (dd, *J* = 8.2, 1.8 Hz, 1H), 9.24 (dd, *J* = 4.3, 1.8 Hz, 1H), 8.82 (dd, *J* = 5.0, 1.6 Hz, 1H), 8.11 (dd, *J* = 7.6, 1.6 Hz, 1H), 7.96 (dd, *J* = 8.1, 4.4 Hz, 1H), 7.53 (dd, *J* = 7.5, 5.0 Hz, 1H), 6.92 (d, *J* = 1.3 Hz, 1H), 6.71 (d, *J* = 1.3 Hz, 1H), 2.72 – 2.56 (m, 3H), 2.40 (s, 3H), 2.37 (d, *J* = 3.5 Hz, 3H), 2.32 (s, 3H).

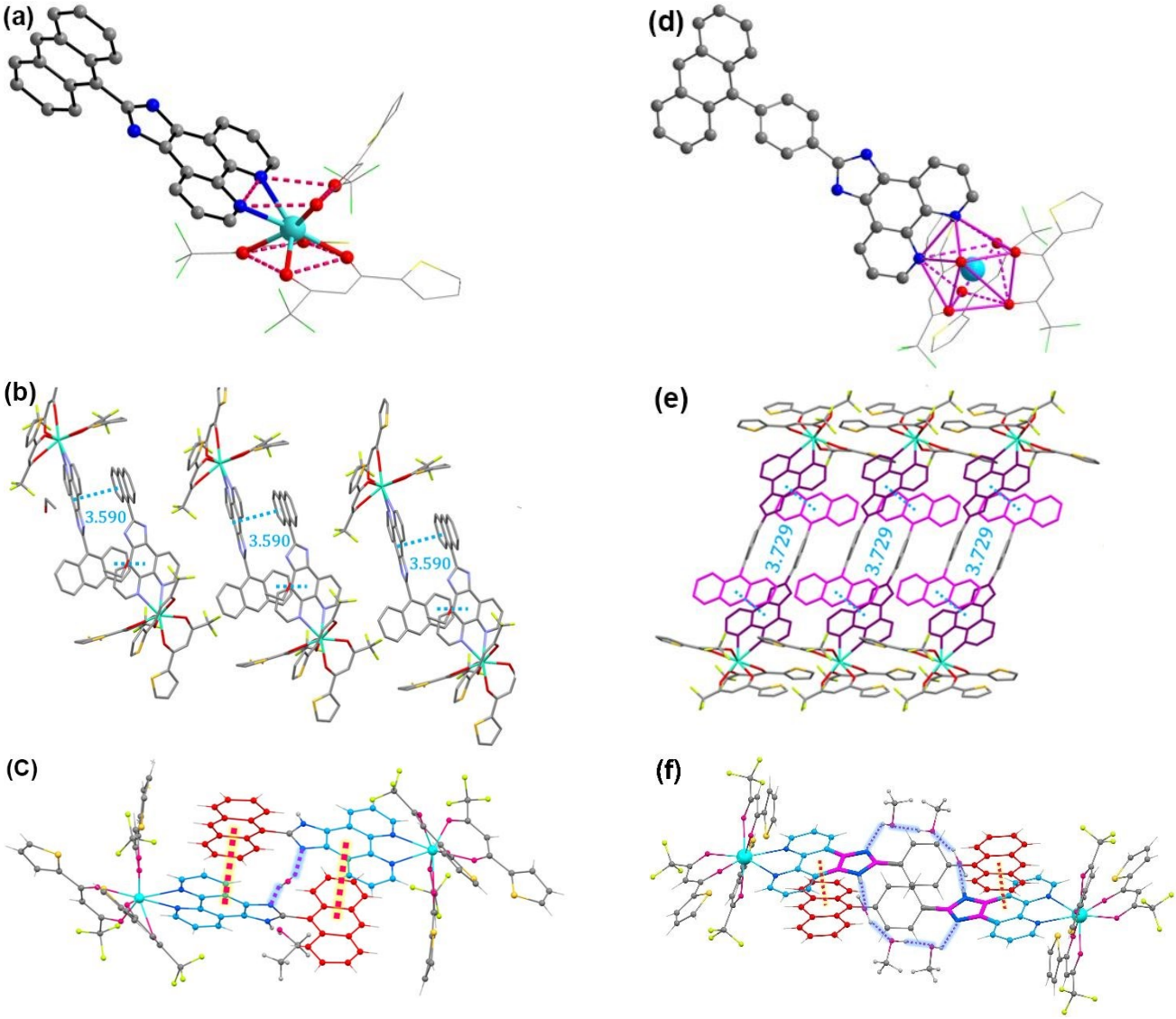

Fig. 1 Crystal structures, polyhedrons around the Dy(III) ions, packing model and hydrogen bonds interaction for **1** (a), (b), (c) and **2** (d), (e), (f). The hydrogen atoms and lattice solvents are omitted for clarity. Colour code: Dy, light-blue; O, red; N, blue; C, grey; F, green; S, yellow. The bottom pictures: along the *a* axis.

View Article Online
DOI: 10.1039/D0DT02864A

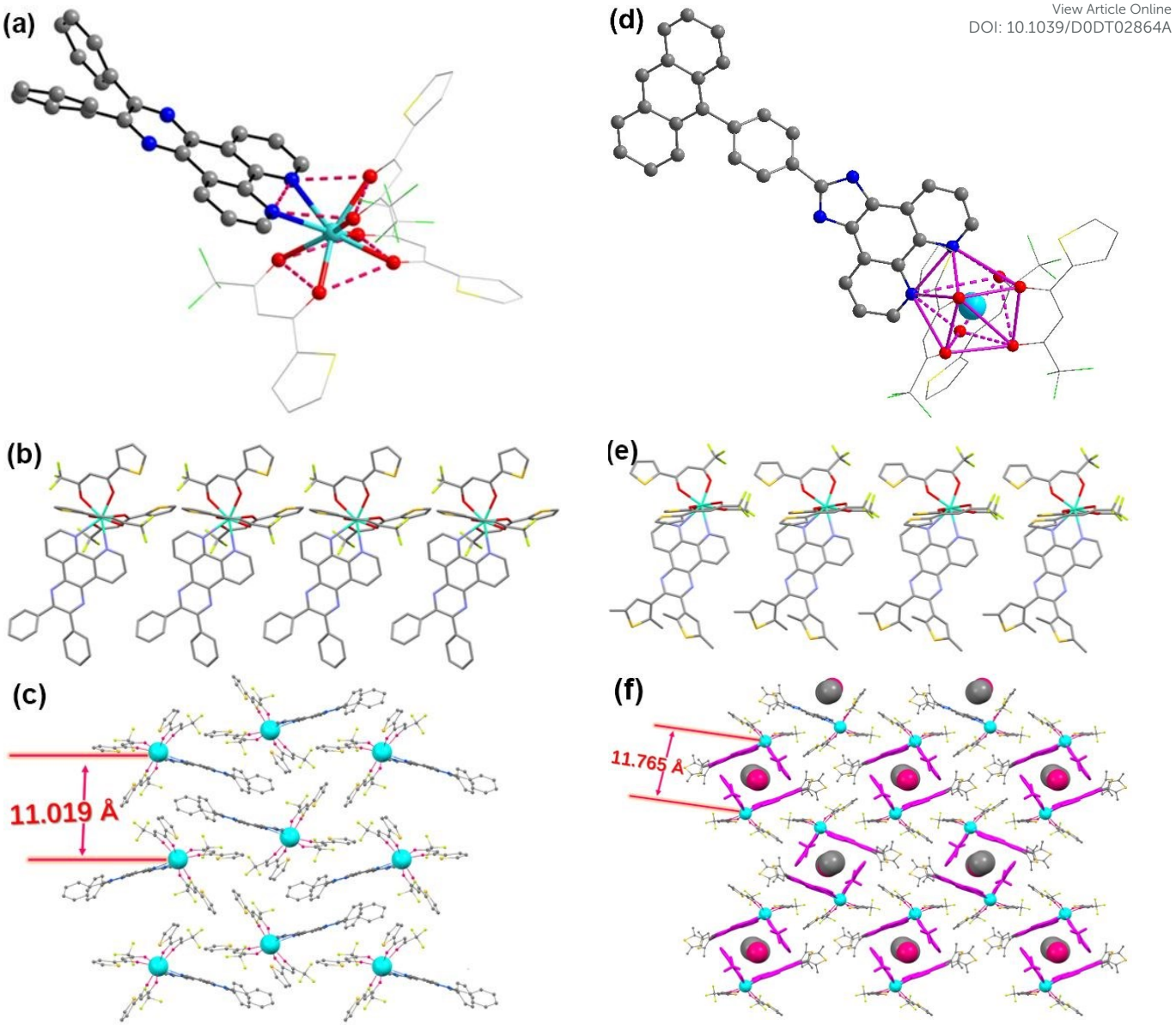

Fig. 2 Crystal structures, polyhedrons around the Dy(III) ions and packing model for **3** (a), (b), (c) and **4** (d), (e), (f). The hydrogen atoms and lattice solvents are omitted for clarity. Color code: Dy, light-blue; O, red; N, blue; C, gray; F, green; S, yellow. The bottom pictures: along the *a* axis

Synthesis of $[Dy^{III}(TTA)_3(AIP)]\cdot 0.5CH_3CH_2OH\cdot 0.5H_2O$ (1), $[Dy^{III}(TTA)_3(DPP)]$ (3) and $[Dy^{III}(TTA)_3(BPP)]\cdot 0.5CH_3CH_2OH$ (4). In a 100 mL round bottom flask, HTTA (0.066 g, 0.3 mmol) and triethylamine (0.067g, 0.6 mmol) were added to 30 mL of ethanol. After 30 minutes of stirring, $Dy(NO)_3\cdot 5H_2O$ (0.044 g, 0.1 mmol) was added and 5 minutes later, the corresponding ligand dissolved in dichloromethane and ethanol was added (AIP: 0.04 g (1 mmol) for **1**), DPP: 0.038 g (1 mmol) for **3** and BPP: 0.045 g (1 mmol) for **4**. The yellow precipitate was collected after stirring overnight. The yellow crystals were obtained by slow evaporation of dissolved precipitate in a mixed solvent of dichloromethane and ethanol with yields of 72%, 81% and 66% respectively. Elemental analysis for $C_{52}H_{32}DyF_9N_4O_7S_3$ (**1**): calculated C, 49.79; H, 2.57; N, 4.47. found C, 49.61; H, 2.65; N, 4.50.$C_{50}H_{28}DyF_9N_4O_6S_3$ (**3**): calculated C, 49.61; H, 2.33; N, 4.63. found C, 49.21; H, 2.12; N, 4.56. $C_{51}H_{35}DyF_9N_4O_{6.5}S_5$ (**4**): calculated C, 47.06; H, 2.71; N, 4.30. found C, 46.55; H, 2.66; N, 4.21.

Synthesis of $[Dy^{III}(TTA)_3(APIP)]\cdot 2CH_3OH\cdot H_2O$ (2). Complex **2** was synthesized similarly to that of **1** as described above and the distinction was just the solvent of ethanol replaced by methanol with yields of 56%. $C_{59}H_{42}DyF_9N_4O_9S_3$ (**2**): calculated C, 51.33; H, 3.07; N, 4.06. found C, 50.99; H, 2.91; N, 4.01.

Synthesis of $[Dy^{III}(TTA)_3(AIP)]\cdot 1.5H_2O$ (5). Complex **5** was synthesized by dissolving crystal sample of complex **1** in ethanol solvent along with addition of two drops of trifluoroacetic acid (TFA) and then slowly evaporated for three days.

Results and discussion

Synthesis and General Characterizations

View Article Online
DOI: 10.1039/D0DT02864A

The title complex was synthesized with the molar ratio of 1:1 by a substitution reaction of intermediate forerunner $Dy(TTA)_3$ with the auxiliary phenanthroline ligand, which was generated by a ring closing reaction with a high yield. The bulk crystal samples of four complexes are all stable in air at room temperature. Furthermore, the purity of the powder samples was characterized by powder X-ray diffraction pattern and the experimental data agree well with the simulated results based on the single-crystal diffraction data (Fig. S1, ESI†).

Crystallography

Single crystals of **1**-**4** can be easily obtained by a method of evaporation of mother solutions. Crystal structures of these four complexes are depicted in Fig. 1 and Fig. 2, respectively. The details of crystallographic refinement parameters are summarized in Table S1†. Those selected bond lengths and bond angles are listed in Table S2† and Table S3†. Four complexes crystallize in monoclinic space group of *C*2/c (**1**), monoclinic space group of $P2_1/c$ (**2**), monoclinic space group of $P2_1/c$ (**3**) and orthorhombic space group of $P2_12_12_1$ (**4**), respectively. The centre eight-coordinated Dy(III) ion is in the coordination environment of $[DyN_2O_6]$, of which six oxygen atoms come from three β-diketones and two nitrogen atoms come from auxiliary ligand. The evaluated local coordination geometry of **2** and **4** is in close proximity to triangular dodecahedron while **1** and **3** is closed to square antiprism with distortion values of 0.506, 1.126, 0.596 and 1.026 by SHAPE software.[32] The Dy-O/N bond lengths are in the range of 2.288-2.345/2.550-2.584 Å (**1**), 2.302-2.337/2.555-2.571 Å (**2**), 2.314-2.347/2.541-2.544 Å (**3**) and 2.288-2.353/2.569-2.590 Å (**4**). The shortest intermolecular Dy···Dy distances are 9.197 (**1**), 10.536 (**2**), 11.019 (**3**) and 11.765 (**4**) Å which are not necessary to preclude any intermolecular interactions between adjacent molecules. For complexes **3** and **4**, adjacent molecules are stacked side by side along *a* axis while for **1** and **2**, the intermolecular π···π stacking interaction between anthracene group and phenanthroline part form the head-to-tail dimers and abreast array with the centroid-to-centroid distances of 3.590 (**3**) and 3.729 (**4**) Å (Fig. 1 and Fig. 2). The imidazole rings as donor and acceptor of hydrogen bonds are linked by lattice solvents between adjacent molecules in complexes **1** and **2**. Driven by π···π stacking interaction, the two neighbour interacted imidazole rings form two hydrogen bonds by means of one bridged water molecule in **1**, while multiple hydrogen bonds by water and methanol molecules make up a circle hydrogen bonds interaction as a result of elongate distance between the two imidazole rings, which is due to the introduction of benzene ring of auxiliary ligand in **2** (Fig. 1). For the six-membered pyrazine ring in complexes **3** and **4**, the hydrogen bond interaction associated with pyrazine ring is absent. However, the obvious hydrogen bonds interaction among ethanol molecules filled in the holes along the *a* axis in complex **4**, makes the shortest intermolecular Dy···Dy distance (11.765 Å) to be longer than it in **3** (11.019 Å) (Fig. 2).

Static Magnetic Properties

The variable-temperature magnetic susceptibilities of four complexes were measured on microcrystalline samples over the temperature range 1.8-300 K under an applied field of 1 kOe. As shown in Fig. 3 and Fig. S2†, at room temperature, the experimentally observed $\chi_m T$ values of 13.91 (**1**), 13.83 (**2**), 13.92 (**3**) and 13.94 (**4**) cm^3Kmol^{-1} are consistent with the expected value of 14.17 cm^3Kmol^{-1} for one independent ground state of Dy(III) ion ($^6H_{15/2}$, $S = 5/2$, $L = 5$, $J = 15/2$, $g = 4/3$).[33] As the temperature decrease, the $\chi_m T$ values decrease gradually until about 50 K and then drops sharply to reach corresponding minimum values of 12.02, 10.17, 11.10 and 9.58 cm^3Kmol^{-1}, which is mainly responsible for the progressive depopulation of excited Stark sublevels and/or weak intermolecular interaction of typical behaviour for Dy(III) ion.[12] As the solid line shown, the fitted results by MOLCAS software are in good accordance with the experimental values. The calculations give the intermolecular interaction *zJ*′ values of −0.001 (**1**), −0.04 (**2**), −0.03 (**3**) and −0.07 (**4**). Furthermore, the variation of magnetization of **1**-**4** are tested at 1.8, 2.5, 5.0 and 10.0 K, respectively. The magnetization *M* versus *H* plots of four complexes at 1.8 K rapidly increases at low field and then reach corresponding maximum values of 5.16, 5.18, 5.14 and 5.16, $N\mu_B$ at 7.0 T, which are far less than the theoretical saturated value of 10 $N\mu_B$ ($g_J \times J$) and indicates well-separated excited Kramers doublets as a result of strong crystal-field splitting.[21,34] The non-superposition of *M* versus *H* plots at different temperatures implies a sign of significant magnetic anisotropy and/or the suggested low-lying excited states. In addition, the magnetization hysteresis as an important characteristic of magnetic bistability was also measured at 1.8 K to verify the slow relaxation of magnetization. As shown in Fig. 3, the M versus *H* plots shows clearly visible butterfly-sharped hysteresis loop for **1** and **4**. All of the above discussions suggest the possibility of SMM property of four complexes.

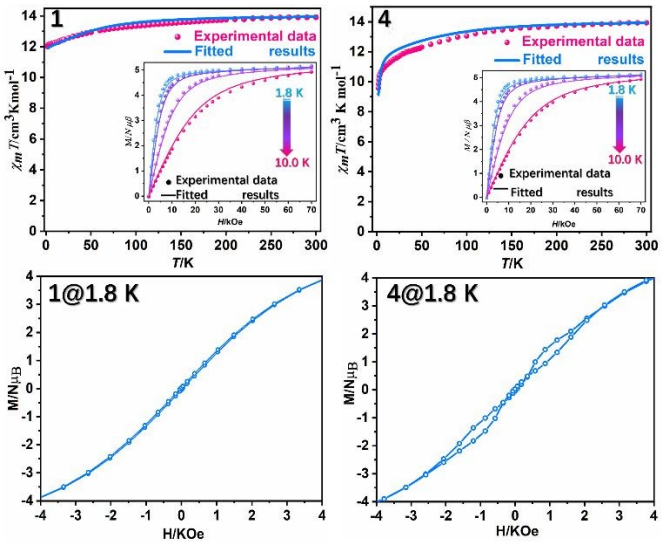

Fig. 3 The variable-temperature magnetic susceptibilities of **1** and **4** under an external field of 1 kOe in the temperature range of 1.8-300 K (top view, insert: field-dependent magnetization at 1.8, 2.5, 5.0 and 10 K. The solid line represents the best fitted results.) and magnetic hysteresis loops for **1** and **4** at 1.8 K under the sweep rate of 200 Oe/s.

Dynamic Magnetic Properties

The dynamic magnetic susceptibility for microcrystalline were measured under zero dc external field to investigate the SMM properties of four complexes. As shown in Fig. 4 and Fig. S3 and S4†, both the frequency- and temperature-dependent in-phase (χ') and out-of-phase (χ'') signals of ac magnetic susceptibilities make the clear attitude of slow relaxation of magnetization. The frequency-dependent out-of-phase (χ'') peaks that demonstrate the "freezing" of the spins by anisotropy barriers move to higher frequency as the increase of temperature at high frequencies region. However, the immobility of out-of-phase (χ'') peaks (Fig. 4) and tails of in-phase (χ') and out-of-phase (χ'') versus T plots among complexes **1**-**4** at low temperature are attributed to the intervention of QTM which rooted in the incomplete blocking of anisotropy barriers and is in response to the mixing of two ground states of degenerate Kramers Dy(III) ions under zero field. In this case, the thermally activated spin reversal is inhabited by a fast temperature-independent quantum relaxation. In the meantime, there is indeed evidence that the relaxation time may distribute in a wide band as a result of the wide peaks of χ'' magnetic susceptibilities. The quasi-semicircles of Cole-Cole plots are fitted by generalized Debye model to give α factors in the range of 0.23-0.18 (1.8-14 K) for **1**, 0.26-0.11 (2.0-19 K) for **2**, 0.13-0.05 (1.8-11 K) for **3** and 0.31-0.09 (1.8-18 K) for **4**, which is consistent with the above analysis of wide distribution of relaxation time. In the high-temperature region, the temperature dependence of relaxation time suggests it to be thermally activated and the extracted magnetic relaxation time τ plotted as a function of $1/T$ that followed an Arrhenius law is fitted the linear experimental data to give the effective energy barriers (Δ/k_B) and pre-exponential factors (τ_0) of 69.4 K and 6.24×10^{-8} s (**1**), 147.3 K and 4.82×10^{-9} s (**2**), 122.1 K and 1.5×10^{-9} s (**3**), 234.2 K and 7.3×10^{-11} s (**4**), respectively. At low temperature, the approximate linear dynamic shows the expected pure quantum regime with τ values of 0.0004 (**1**), 0.002 s (**2**), 0.0008 (**3**) 0.003 (**4**) which indicates a relatively faster relaxation of **1** and **3** than **2** and **4**, and consistent with the experimentally determined effective energy barriers (see ESI†).

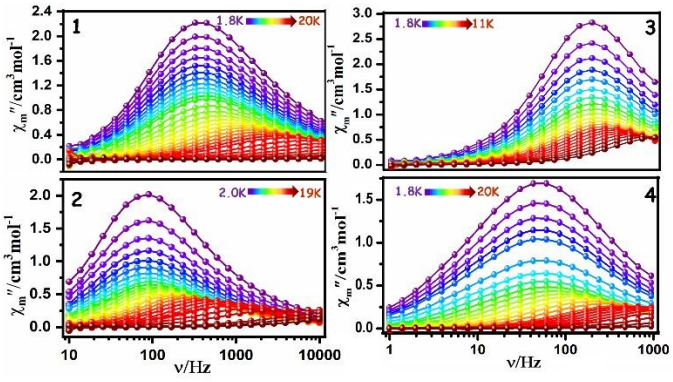

Fig. 4 Frequency dependence of the out-of-phase (χ'') ac susceptibility of **1**, **2**, **3** and **4** in zero dc field.

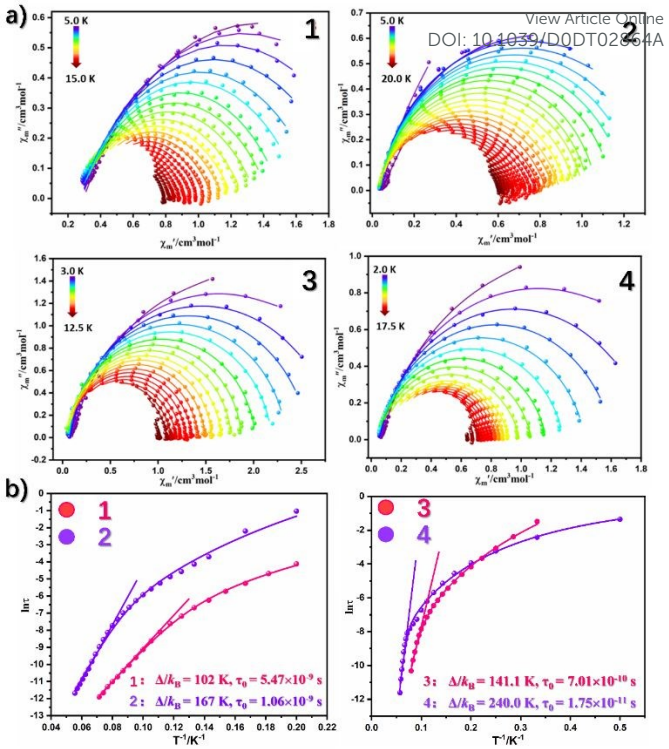

Fig. 5 a) The Cole-Cole fitted data for **1**, **2**, **3** and **4** under the optimal field (800 (**1**), 1000 (**2**), 1500 (**3**) and 1000 (**4**) Oe) by generalized Debye model (the solid lines represent the best results). b) The extracted magnetic relaxation time τ plot as a function of $1/T$ of four complexes under the optimal field. The straight lines represent data fitting with Arrhenius law and the curves lines represent the best fitting based on eq. 1.

In general, external magnetic field can be applied to effectively suppress the QTM process.[23] The ac magnetic susceptibilities under different external fields were detected to search an optimal field and the χ'' versus H were recorded with varying applied fields. The significant signals of maximal value at the magnetic fields of 1500 (**1**), 1000 (**2**), 1000 (**3**) and 800 Oe (**4**) represent an instruction of field-induced magnetization and the slowest relaxation, thus these external magnetic field were selected as the optimal field to suppress the QTM process. As the Fig. S5† shows, the rising tails of in-phase (χ') and out-of-phase (χ'') versus T plots disappear apparently at low temperatures by reference to that in zero field plot and show obvious shift to high temperature as the increase of frequency. These phenomena indicate that the QTM is indeed effectively suppressed. The magnetic relaxation time τ are extracted according to the corresponding Cole-Cole fitting. The thermal activated energy barriers of 102.0 K (**1**), 167.0 K (**2**), 141.1 K (**3**) and 240.0 K (**4**) are achieved by fitting the high-temperature experimental data using Arrhenius law. Furthermore, the multiple relaxation processes of Direct, Raman and Orbach are taken into account using **eq. 1** to clarify the whole behaviours in the ln(τ) vs $1/T$ plots. The best fitted parameters were obtained, that is, A = 1.1 $s^{-1}K^{-1}$, C = 0.0095 $s^{-1}K^{-5.45}$, n = 5.45, τ_0 = 5.47×10^{-9} s, Δ/k_B = 102.0 K (**1**); A = 0.05 $s^{-1}K^{-1}$, C = 0.0001 $s^{-1}K^{-6.51}$, n = 6.51 τ_0 = 1.06×10^{-9} s, Δ/kB = 167.0 K (**2**) A = 0.001 $s^{-1}K^{-1}$, C = 0.025 $s^{-1}K^{-4.84}$, n = 4.84, τ_0 = 7.01×10^{-10} s, Δ/k_B = 141.1 K (**3**); A = 1.11 $s^{-1}K^{-1}$, C = 0.12 $s^{-1}K^{-3.75}$, n = 3.75, τ_0 = 1.75×10^{-11} s, Δ/k_B = 240.0 K (**4**).

$$\tau^{-1} = AT + CT^n + \tau_0^{-1}\exp(-\Delta/k_BT) \quad (1)$$

The dynamic magnetic studies reveal the significant difference among four complexes, which indicates the distinct influence of the ligand field on various relaxation mechanisms. The analysis of X-ray single crystal structure shows that the slight changes of the ligand can lead to transformation of the local geometrical configuration of the Dy(III) centre and thus regulate the slow magnetic relaxation. What was known is that the different local symmetry and coordination bond distance can bring an effectively influence on the ligand fields, which frankly give rise to diverse magnetic behaviours. Nevertheless, the novel magnetic anisotropy is dominated not only by local symmetry, but also by simultaneously complicated factors such as, electrostatics, guest molecules and delocalization effect of neutral ligand. Therefore, in-depth theoretical explorations of magneto-structural correlations are full of worth.

Ab Initio Calculations

For a better theoretical elucidation of the prominent difference of magnetic properties of four complexes, the CASSCF calculations based on X-ray single crystal structures have been performed on individual Dy(III) fragment for each complex through MOLCAS 8.4 and SINGLE_ANISO programs. The computational results are presented in the Supporting Information in detail. The calculated lowest spin-orbit energies and the correlative ***g*** tensors manifest the strong axial anisotropy of the ground KD with *g* values: g_x = 0.025, g_y = 0.036, g_z = 19.517 (m_J = ±15/2, **1**); g_x = 0.009, g_y = 0.010, g_z = 19.458 (m_J = ±15/2, **2**); g_x = 0.017, g_y = 0.024, g_z = 19.561 (m_J = ±15/2, **3**); g_x = 0.004, g_y = 0.007, g_z = 19.640 (m_J = ±15/2, **4**). In spite of higher than previous reported results of high-performed Dy(III)-SIM, such small g_x and g_y suggested the nominal criterion for slow magnetic magnetization in zero field of four complexes.[17,18] The predominant m_J values of the ground states and first excited states are mostly composed by ±15/2 and ±13/2 for four complexes (Table 1). The distinct differences of ***g*** tensors put forward to the conclusion that complex **4** possesses more Ising-type axial anisotropy of ground doublets than **3**. In accordance with the calculated results of the first excited energy, the experimental energy barriers of 102.0 K (**1**), 167.0 K (**2**), 141.1 K (**3**) and 240.0 K (**4**) are closed to the theoretically calculated results of 148.2 K (**1**), 187.5 K (**2**), 166.9 K (**3**) and 225.5 K (**4**). The much smaller shortcut value of the experimental datum of 69.4 K in zero dc field than the calculated value of 148.2 K for **1** suggests that such a relaxation does not reach the first excited state in this complex due to fast under-barrier relaxation caused by anharmonic phonons.

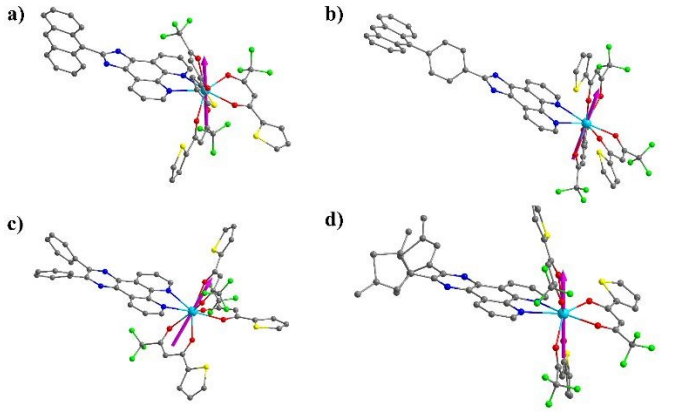

Fig. 6 The ab initio calculated orientations of the local main magnetic axes of the ground KDs on Dy(III) ions for complexes **1** (a), **2** (b), **3** (c) and **4** (d), respectively. Colour code: Dy, light-blue; O, red; N, blue; C, grey; F, green; S, yellow.

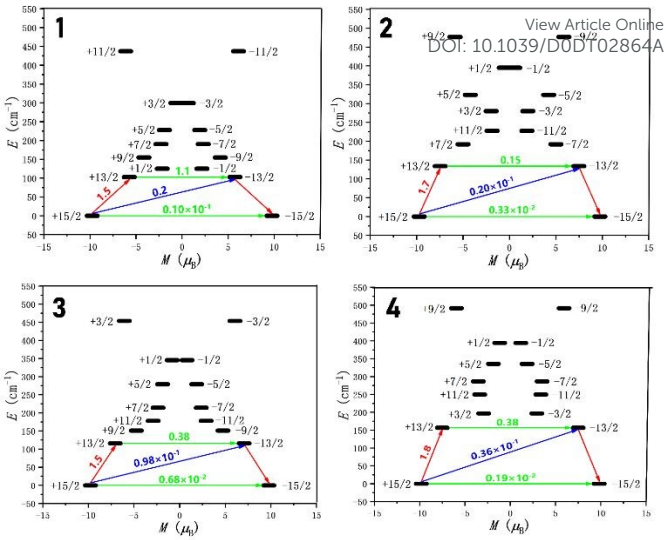

Fig. 7 The Magnetization blocking barriers in **1**, **2**, **3** and **4**, respectively. The thick black lines represent the KDs as a function of their magnetic moments along the magnetic axis. The green lines correspond to diagonal QTM, and the blue lines represent Orbach relaxation process. The red arrows represent the most possible path for magnetic relaxation. The numbers at each arrow stand for the mean absolute values of the transversal magnetic moments.

Based on the theoretically calculated orientation of the magnetic easy axis (Fig. 6), those planes containing two nitrogen atoms of auxiliary ligands that are vested in the equatorial plane assume to be nearly perpendicular to the main magnetic axis. The above studies have essentially determined the more axial of KDs in **2** (**4**) than **1** (**3**). Previously reported results have shown the preference of excess of axial electrostatic repulsion of high-performance SMMs around the central Dy(III) ions. As a result, the more charge distribution in the equatorial plane has the opposite effect. The slightly larger values of NBO charge on coordinated nitrogen atoms in **3** (**1**) than **4** (**2**) seemingly shows the variant electron donor effect and the influence on electrostatic potential in equatorial plane (Fig. S17†). So, the almost twofold higher effective energy barrier of **4** than that of **3** is mainly originates from the stronger conjugation effects of

Table 1. Wave functions with definite projection of the total moment | m_J > for the lowest two KDs for complexes **1**, **2**, **3** and **4**.

	E/cm^{-1}	wave functions
1	0.0	94.9%|±15/2>
	102.9	46.7%|±13/2>+11.2%|±3/2>+11.1%|±11/2>
2	0.0	93.0%|±15/2>
	133.9	57.6%|±13/2>+27.1%|±9/2>+9.4%|±11/2>
3	0.0	95.2%|±15/2>
	115.9	55.0%|±13/2>+15.8%|±11/2>+13.8%|±9/2>
4	0.0	95.2%|±15/2>
	156.6	71.9%|±13/2>+16.0%|±9/2>

benzene rings than thiophene rings and furtherly enhance electrostatic potential in equatorial plane.[35] As a consequence, the Dy-N bond distances of **4** are longer than **3**. For complex **2**, the anthracene group and phenanthroline group in the ligand are isolated by the intermediate benzene group, which resulting in the nearly orthorhombic configuration between anthracene and benzene rings with a dihedral angle of 59.44°, and resistance effect for charge flowing. Naturally, **2** take possession of relatively less electrostatic potential than **1** in equatorial plane, which conforms to both the experimental data and *ab initio* calculations (see ESI†). However, the role of intermolecular hydrogen bonds interactions should be the dominant factor in modulating the magnetic dynamic of **1** and **2** by contrasting with the impact of electrostatic potential. Fabrice Pointillart [23d,23e] has revealed that the hydrogen bond interaction in non-alkylated imidazole ring result in the absence of SMM property. By comparing the experimental energy barrier of **1** with **2**, the depravation of SMM property in **1** may be on account of the distinct intermolecular hydrogen bonds that are made up of only two O_{H_2O}-H···$N_{imidazole}$ interactions between adjacent molecules, than **2** whose hydrogen bonds form a circulation by feat of multiple $N_{imidazole}$-H···O_{H_2O}, O_{H_2O}-H···O_{CH_3OH}, O_{CH_3OH}-H···O_{CH_3OH} and O_{CH_3OH}-H···$N_{imidazole}$ interactions (Fig. 2). To elucidate the speculation of hydrogen bond influence, complex **5** with main structure similar to **1** has been synthesized by dissolving complex **1** in ethanol solvent along with addition of two drops of trifluoroacetic acid (TFA) (see ESI†). As shown in Fig. S10†, the lattice solvent of **5** was only water while water and ethanol molecules were found in **1**. Meanwhile, the hydrogen bond interactions display distinct modes. In **5**, all the N and H atoms located in imidazole ring form $N_{imidazole}$-H···O_{H2O} or $N_{imidazole}$···H-O_{H2O} hydrogen bonds. However, only one type of hydrogen bond interaction exists in **1**. Furthermore, the coordination bond distances are slightly variable (Table S17†). Thus, complex **5** have the nearly identical structure with **1** except for the intermolecular hydrogen bond interaction. As shown in Figs. S13 and S14†, the independence of out-of-phase (χ'') versus ν and tails of out-of-phase (χ'') versus T plots of **1** and **5** at low temperature indicates the presence of strong QTM. However, the peaks of out-of-phase (χ'') in the lower frequency regions of **5** demonstrates the slower magnetic relaxation than **1**. The magnetic energy barriers of 45.0 K (**1**) and 70.6 K (**5**) are achieved by fitting the high-temperature data using Arrhenius law. The pure quantum regime with τ values are 0.0003 (**1**) and 0.0006 (**5**), which indicates the relatively faster relaxation in **1** (Figs. S15 and S16†). From these results, it is suggested that after dealing with TFA, the new complex **5**, with distinct hydrogen bond interaction comparing with **1** shows modest improvement of SMM property. We then perform a theoretical CASSCF calculation of **5** through MOLCAS 8.4 with the same method as **1** for comparison. The calculated results are shown in Table S18 and S19, Figs. S17 and S18†. It is obvious that the calculated parameters of **5** are nearly the same as **1**, which accounts for the nearly same coordination environment. Therefore, the experimental difference of magnetic dynamic can be ascribed to the distinction of hydrogen bond interactions. Based on the experimental and theoretical analyses, we point out that in this system the hydrogen bond interactions play an important role in manipulating magnetic dynamic.

Conclusions

View Article Online
DOI: 10.1039/D0DT02864A

In summary, we have synthesized five new eight-coordinate Dy-β-diketones complexes of **1**, **2**, **3**, **4** and **5** by modulating auxiliary ligand. They all perform as SIMs with Ising-type ground states and demonstrate that stronger electron conjugation effect of auxiliary ligands and intermolecular hydrogen bonds interactions results in deterioration of magnetic anisotropic barriers. The further in-depth research of relaxation mechanism was elucidated by cooperating experiment with theoretical studies, as a result of which the diverse SIM behaviours with various degree of QTM process are responsible for the subtle modification of coligands. In this work, we demonstrate that the slight modulating of the auxiliary ligand can not only regulate charge conjugation effect, but also simultaneously change the local symmetry of Dy(III) ion and intermolecular interactions, by which generate the variation of energy sublevels to bring different dynamic magnetic behaviours into existence. Overall, we provide a fresh perspective in certifying the authenticity and significance of electron-donating effect and intermolecular interactions of auxiliary ligand for modulating the magnetic properties.

Conflicts of interest

There are no conflicts to declare.

Acknowledgements

We thank the National Key R&D Program of China (2017YFA0303203 and 2018YFA0306004) and the National Natural Science Foundation of China (21571097, 21973038 and 21973046).

Notes and references

1 (a) D. N. Woodruff, E. P. Winpenny and R. A. Layfield, *Chem. Rev.*, 2013, **113**, 5110. (b) P. Zhang, L. Zhang and J. Tang, *Dalton Trans*., 2015, **44**, 3923. (c) S. T. Liddle, and J. van Slageren, *Chem. Soc. Rev.*, 2015, **44**, 6655. (d) J. Tang and P. Zhang, Lanthanide Single Molecule Magnets; Springer Berlin Heidelberg: Berlin, Heidelberg, 2015.
2 (a) Y.-S. Meng, S.-D. Jiang, B.-W. Wang and S. Gao, *Acc. Chem. Res.*, 2016, **49**, 2381. (b) R. A. Layfield and M. Murugesu, Lanthanides and actinides in molecular magnetism; John Wiley & Sons: Weinheim, Germany, 2015.
3 (a) J. D. Rinehart and J. R. Long, *Chem. Sci*., 2011, **2**, 2078. (b) J. Luzon and R. Sessoli, *Dalton Trans.*, 2012, **41**, 13556. (c) F.-S. Guo, A. K. Bar and R. A. Layfield, *Chem. Rev.*, 2019, **119**, 8479. (d) O. Cador, B. Le Guennic and F. Pointillart, *Inorg. Chem. Front.*, 2019, **6**, 3398. (e) L. Spree and A. A. Popov, *Dalton Trans.*, 2019, **48**, 2861.
4 C. A. P. Goodwin, F. Ortu, D. Reta, N. F. Chilton and D. P. Mills, *Nature*, 2017, **548**, 439.
5 F. S. Guo, B. M. Day, Y.-C. Chen, M.-L. Tong, A. Mansikkamäki and R. A. Layfield, *Science*, 2018, **362**, 1400.
6 M. N. Leuenberger and D. Loss, *Nature*, 2001, **410**, 789.
7 L. Bogani and W. Wernsdorfer, *Nat. Mater.*, 2008, **7**, 179.
8 M. Atzori and R. Sessoli, *J. Am. Chem. Soc.*, 2019, **141**, 11339.
9 F. Liu, L. Spree, D. S. Krylov, G. Velkos, S. M. Avdoshenko and A. A. Popov, *Acc. Chem. Res.*, 2019, **52**, 2981.

10 A. Albino, S. Benci, L. Tesi, M. Atzori, R. Torre, S. Sanvito, R. Sessoli and A. Lunghi, *Inorg. Chem.*, 2019, **58**, 10260.
11 J.-L. Liu, Y.-C. Chen and M.-L. Tong, *Chem. Soc. Rev.*, 2018, **47**, 2431.
12 G.-J. Chen, Y. N. Guo, J.-L. Tian, J. Tang, W. Gu, X. Liu, S. P. Yan, P. Cheng and D. Z. Liao, *Chem. Eur. J.*, 2012, **18**, 2484.
13 D. Aravena and E. Ruiz, *Inorg. Chem.*, 2013, **52**, 13770.
14 (a) P.-P. Chen, S. Zhang, X.-Y. Liu, W.-M. Song, Y.-Q. Zhang, G. Xie and S.-P. Chen, *Inorg. Chem.*, 2017, **56**, 3644. (b) D. Errulat, R. Marin, D. A. Gálico, K. L. M. Harriman, A. Pialat, B. Gabidullin, F. Iikawa, O. D. D. Couto Jr., J. O. Moilanen, E. Hemmer, F. A. Sigoli and M. Murugesu, *ACS Cent. Sci.*, 2019, **5**, 1187.
15 J. Wu, O. Cador, X.-L. Li, L. Zhao, B. Le Guennic and J. Tang, *Inorg. Chem.*, 2017, **56**, 11211.
16 (a) S. Bala, G.-Z. Huang, Z.-Y. Ruan, S.-G. Wu, Y. Liu, L.-F. Wang, J.-L. Liu and M.-L. Tong, *Chem. Commun.*, 2019, **55**, 9939. (b) F. Guégan, J. Jung, B. Le Guennic, F. Riobé, O. Maury, B. Gillon, J.-F. Jacquot, Y. Guyot, C. Morell and D. Luneau, *Inorg. Chem. Front.*, 2019, **6**, 3152. (c) S. Zhang, W. Mo, J. Zhang, Z. Zhang, B, Yin, D. Hu and S. Chen, *Inorg. Chem.*, 2019, **58**, 15330. (d) L. Sun, S. Zhang, C. Qiao, S. Chen, B. Yin, W. Wang, Q. Wei, G. Xie and S. Gao, *Inorg. Chem.*, 2016, **55**, 10587.
17 Y.-C. Chen, J.-L. Liu, L. Ungur, J. Liu, Q.-W. Li, L.-F. Wang, Z.-P. Ni, L. F. Chibotaru, X.-M. Chen and M.-L. Tong, *J. Am. Chem. Soc.*, 2016, **138**, 2829.
18 J. Liu, Y.-C. Chen, J.-L. Liu, V. Vieru, L. Ungur, J.-H. Jia, L. F. Chibotaru, Y. Lan, W. Wernsdorfer, S. Gao, X.-M. Chen and M.-L. Tong, *J. Am. Chem. Soc.*, 2016, **138**, 5441.
19 A. B. Canaj, S. Dey, E. R. Martí, C. Wilson, G. Rajaraman and M. Murrie, *Angew. Chem. Int. Ed.*, 2019, **58**, 14146.
20 Z. H. Li, Y. Q. Zhai, W. P. Chen, Y. S. Ding and Y. Z. Zheng, *Chem. Eur. J.*, 2019, **25**,16219.
21 (a) N. Ishikawa, M. Sugita, T. Ishikawa, S. Koshihara and Y. Kaizu, *J. Am. Chem. Soc.*, 2003, **125**, 8694. (b) Y. Bi, Y.-N. Guo, L. Zhao, Y. Guo, S.-Y. Lin, S.-D. Jiang, J. Tang, B.-W. Wang and S. Gao, *Chem. Eur. J.*, 2011, **17**, 12476. (c) J. Wu, J. Jung, P. Zhang, H. Zhang, J. Tang and B. Le Guennic, *Chem. Sci.*, 2016, **7**, 3632.
22 D.-P. Li, T.-W. Wang, C.-H. Li, D.-S. Liu, Y.-Z. Li and X.-Z. You, *Chem. Commun.*, 2010, **46**, 2929.
23 (a) S.-D. Jiang, B.-W. Wang, G. Su, Z.-M. Wang and S. Gao, *Angew. Chem. Int. Ed.*, 2010, **49**, 7448. (b) S. Zhang, H. Ke, L. Sun, X. Li, Q. Shi, G. Xie, Q. Wei, D. Yang, W. Wang and S. Chen, *Inorg. Chem.*, 2016, **55**, 3865. (c) J. F. Gonzalez, F. Pointillart and O. Cador, *Inorg. Chem. Front.*, 2019, **6**, 1081. (d) G. Cosquer, F. Pointillart, S. Golhen, O. Cador and L. Ouahab, *Chem. Eur. J.*, 2013, **19**, 7895. (e) J. Jung, O. Cador, K. Bernot, F. Pointillart, J. Luzon and B. Le Guennic, *Beilstein J. Nanotechnol.*, 2014, **5**, 2267.
24 M. Guo, J. Wu, O. Cador, J. Lu, B. Yin, B. Le Guennic and J. Tang, *Inorg. Chem.*, 2018, **57**, 4534.
25 (a) S. Oh, J. R. Gallagher, J. T. Miller and Y.S. Surendranath, *J. Am. Chem. Soc.*, 2016, **138**, 1820. (b) B. M. Neilson, V. M. Lynch and C. W. Bielawski, *Angew. Chem. Int. Ed.*, 2011, **50**, 10322.
26 Y. Teki, S. Miyamoto, M. Nakatsuji and Y. Miura, *J. Am. Chem. Soc.*, 2001, **123**, 294.
27 SAINT-Plus, version 6.02; Bruker analytical X-ray system: Madison, WI, 1999.
28 G. M. Sheldrick, SADABS an empirical absorption correction program; Bruker Analytical X-ray Systems: Madison, WI, 1996.
29 G. M. Sheldrick, *Acta Crystallogr., Sect. A: Found. Crystallogr.*, 2008, **A64**, 112.
30 E. A. Boudreaux and L. N. Mulay , Theory and Applications of Molecular Paramagnetism, John Wiley & Sons, New York, 1976.
31 (a) F. Aquilante, J. Autschbach, R. K. Carlson, L. F. Chibotaru, M. G. Delcey, L. De Vico, I. F. Galván, N. Ferré, L. M. Frutos, L. Gagliardi, M. Garavelli, A. Giussani, C. E. Hoyer, G. Li Manni, H. Lischka, D. Ma, P. Å. Malmqvist, T. Müller, A. Nenov, M. Olivucci, T. B. Pedersen, D. Peng, F. Plasser, B. Pritchard, M. Reiher, I. Rivalta, I. Schapiro, J. Segarra-Martí, M. Stenrup, D. G. Truhlar, L. Ungur, A. Valentini, S. Vancoillie, V. Veryazov, V. P. Vysotskiy, O. Weingart, F. Zapata and R. Lindh, *J. Comput. Chem.*, 2016, **37**, 506. (b) L. F. Chibotaru, Theoritical understanding of anisotropy in molecular nanomagnets, *Struc. Bonding (Berlin, Ger.)* 2014, **164**, 185. (c) L. Ungur and L. F. Chibotaru, *Inorg. Chem.*, 2016, **55**, 10043. (d) J. J. Baldoví, Y. Duan, R. Morales, A. Gaita-Ariño, E. Ruiz and E. Coronado, *Chem.Eur. J.*, 2016, **22**, 13532. (e) L. Ungur and L. F. Chibotaru, *Phys. Chem. Chem. Phys.*, 2011, **13**, 20086. (f) L. F. Chibotaru and L. Ungur, *J. Chem. Phys.*, 2012, **137**, 064112. (g) D. Aravena, *J. Phys. Chem. Lett.*, 2018, **9**, 5327. (h) L. Llanos and D. Aravena, *J. Magn. Magn. Mater.*, 2019, **489**, 165456. (i) B. Yin and C.-C. Li, *Phys. Chem. Chem. Phys.*, 2020, **22**, 9923. (j) A. Castro-Alvarez, Y. Gil, L. Llanos and D. Aravena, *Inorg. Chem. Front.*, 2020, **7**, 2478. (k) D. Aravena and E. Ruiz, *Dalton Trans.*, 2020, **49**, 9916.
32 D. Casanova, M. Llunell, P. Alemany and S. Alvarez, *Chem. Eur. J.*, 2005, **11**, 1479.
33 (a) J. Li, S. Gómez-Coca, B. S. Dolinar, L. Yang, F. Yu, M. Kong, Y.-Q. Zhang, Y. Song and K. R. Dunbar, *Inorg. Chem.*, 2019, **58**, 2610. (b) J. Li, C. Yuan, L. Yang, M. Kong, J. Zhang, J.-Y. Ge, Y.-Q. Zhang and Y. Song, *Inorg. Chem.*, 2017, **56**, 7835.
34 Y. Gao, G.-F. Xu, L. Zhao, J. Tang and Z. Liu, *Inorg. Chem.*, 2009, **48**, 11495.
35 X.-W. Liu, Z. Wu, J.-T. Chen, L. Li, P. Chen and W.-B. Sun, *Inorg. Chem. Front.*, 2020, **7**, 1229.

View Article Online
DOI: 10.1039/D0DT02864A

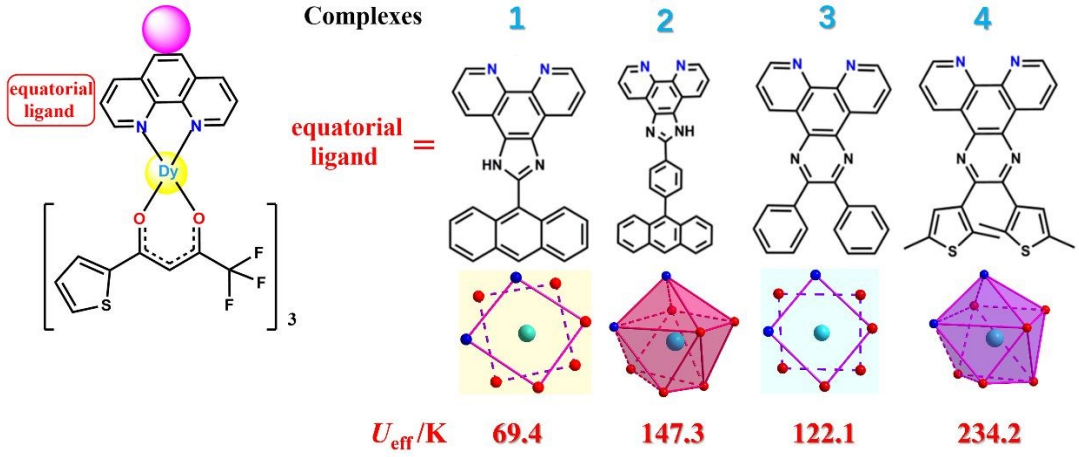

Four perturbed eight-coordinated mononuclear β-diketone based Dy(III) SIMs with distinct hydrogen bonds interaction and electron delocalization are noteworthily modulated by the aromatous groups of auxiliary ligands.